# Chapter 3 : Structural, Optical, and Temperature Sensing Comparison of $Er^{3+}/Yb^{3+}$ co-doped $CaMoO_4$ phosphors in bulk and nanostructure forms.

## 3.1 Introduction

Chapter 1 discussed the importance of using lanthanide-doped materials in optical applications, especially for temperature sensing and latent fingerprint detection. The unique electronic configurations of lanthanide ions, particularly their 4f-4f transitions, allow for developing highly efficient luminescent materials with adjustable optical properties. In particular, we highlighted the $Er^{3+}/Yb^{3+}$ ion pair for its intense upconversion (UC) luminescence, where it converts infrared radiation into visible light, making it ideal for sensing applications. Lanthanide-doped phosphors, like $CaMoO_4$, have excellent thermal and chemical stability and are effective matrices for incorporating these dopants to achieve improved luminescent properties.

In Chapter 2, we examined different synthesis techniques used to create Erbium ($Er^{3+}$) and Ytterbium ($Yb^{3+}$) -doped $CaMoO_4$ phosphors, as well as their structural, optical, and morphological characteristics. The solid-state reaction, sol-gel combustion, and hydrothermal methods were employed to synthesize bulk and nanostructured phosphors. This wide array of synthesis methods allowed for comparing the properties of bulk and nano phosphors, especially in their optical emission behavior and temperature sensing capabilities.

Building on the foundation established in the previous chapters, this chapter delves into the application of $Ca_{0.79}Er_{0.01}Yb_{0.2}MoO_4$ phosphor for temperature sensing, explicitly comparing the performance of bulk and nanostructured phosphors. Lanthanide activators ($Ln^{3+}$) are known for their unique optical properties such as high colour purity, lesser disturbance of the excited states by crystal field surroundings, long excited-state lifetimes, and the up-conversion

and down-conversion emission, etc. Owing to the above attributes, lanthanide-doped phosphors are ideal optical materials for several applications including optical temperature sensing [109]. Various types of temperature measuring techniques have been developed so far, however, lanthanide luminescence-based optical temperature sensors play a very vital character in terms of contactless sensing, non-invasive, and of high sensitivity, etc., [74]. The change in the external temperature of the lanthanide doped phosphors may imply different types of changes in their spectroscopic properties such as change in the overall emission intensity, variation in relative emission intensities of different transition or luminescence kinetics, etc. [75]. Optical temperature sensing can be realized by making use of any one of these spectroscopic changes with temperature.

Optical properties of the lanthanide doped phosphors also rely on different parameters such as particle size/shape, site symmetry around lanthanide ion, and on the statistical distribution of the active ions in them [110]. For example, an enhancement in UC emission intensity and the efficiency with increase of the particle size is already reported [111]. However, a comprehensive study on the effect of bulk and its nano-particles on the temperature sensing ability of the lanthanide doped phosphor is rarely reported. Herein, the synthesis method plays a crucial role in controlling the shape and size of the particles [112]. The particle size of the synthesized phosphors is further affected by calcination of the phosphor material at various temperatures also [113].

In the present work, we have synthesized $Er^{3+}/Yb^{3+}$ co-doped $CaMoO_4$ phosphors in bulk and nanostructure by two different synthesis techniques i.e., by solid-state reaction and gel-combustion method, respectively. A comparative structural and optical properties have been studied for both the bulk and the nanoparticles of $Er^{3+}/Yb^{3+}$ co-doped $CaMoO_4$ phosphors.

XRD, SEM, and TEM characterizations have been performed for the structural analysis. While, FTIR, UV-Visible absorption, photoluminescence emission/excitation, upconversion emission characterizations have been carried-out in detail for the study of optical properties. Finally, the optical temperature sensing by both types of phosphors have been done in the temperature range (305 K - 573 K) and compared. Our study shows that, the sensitivity of the $Ca_{0.79}Er_{0.01}Yb_{0.2}MoO_4$ synthesized by combustion method (CCEY) is comparatively better than $Ca_{0.79}Er_{0.01}Yb_{0.2}MoO_4$ synthesized by solid-state reaction method (SCEY).

## 3.2 Synthesis

### 3.2.1 Solid-state reaction synthesis

Synthesis of the pure and $Er^{3+}/Yb^{3+}$ co-doped $CaMoO_4$, i.e., $Ca_{1-x-y}Er_xYb_yMoO_4$, where x=0, 0.004, 0.007, 0.01, 0.012 and 0.015 with fixed y=0, 0.20. For the synthesis, a stoichiometric amount of precursor powders was taken and mixed properly for 2 h by mortar and pestle. The powder was then calcined in a high-temperature muffle furnace maintained at 1200 °C for 3 h (heating rate-5 °C/min). The synthesized samples were further grounded to get homogeneous powder for further characterizations.

### 3.2.2 Combustion synthesis

The phosphor $Ca_{0.79}Er_{0.01}Yb_{0.2}MoO_4$ synthesised through the solid-state reaction route was found to be optimal with respect to UC emission intensity. The stoichiometric phosphor was also synthesized by gel-combustion route [114]. Initially, the stoichiometric amount of the CaO, $Er_2O_3$, and $Yb_2O_3$ were taken separately in a beaker. Then, 3-4 ml of nitric acid added into it dropwise and the solution is magnetically stirred with 200 rpm on a hot plate maintained at a temperature 100 $^{o}$C to get a transparent solution. Further, 1 ml deionised (DI) water was

added in the solution for complete elimination of nitric acid. In another beaker, stoichiometric ammonium molybdate was mixed with 30 ml DI water with continuous stirring at 30 $^{\circ}$C. After 15 minutes, when the solution became transparent, 2 mg urea was added in it and the temperature is elevated to 85 $^{\circ}$C. After 15 minutes, all the individually prepared solutions were mixed in a beaker which was further kept at a hot plate maintained 200 $^{\circ}$C under constant stirring until dehydration happens and the solution becomes gel-like. Finally, temperature is elevated to 450 $^{\circ}$C and the stirring is stopped. This leads to persistent heating and thus auto-ignition takes place, giving a voluminous fluffy power of phosphor.

Three samples namely pristine $CaMoO_4$ power synthesized using solid state reaction method (hereafter referred as SCM), $Ca_{0.79}Er_{0.01}Yb_{0.2}MoO_4$ power synthesized using solid state reaction method (hereafter referred as SCEY) and through solution combustion method (hereafter referred as CCEY) were used for comparative studies of different properties.

## 3.3 Results and Discussion

### 3.3.1 X-ray diffraction and TEM/SEM measurement: Phase and structure analysis

The XRD patterns of the $Ca_{0.79}Er_{0.01}Yb_{0.2}MoO_4$ powder synthesized using solution combustion method and conventional solid-state reaction route i.e., CCEY and SCEY, are compared with the XRD pattern of pristine $CaMoO_4$ powder synthesized using solid state reaction method (SCM), as shown in Fig 3.1(a). The overlapping diffraction peaks of all three samples confirm that the crystal structure remains unchanged regardless of synthesis route or dopant inclusion. All three samples exhibit a tetragonal phase with space group $I4_1/a$, matched with the standard JCPDS card number 01-085-0585. XRD pattern of the as-synthesized

$CaMoO_4$ power sample synthesized through solid state reaction route (SCM) is in good agreement with the previously reported data [29][30][31]. The $CaMoO_4$ forms tetragonal structure with the space group $I4_1/a$ matched with joint committee on powder diffraction standard (JCPDS card number: 01-085-0585). The well-defined sharp diffraction peaks confirm the good crystallinity of the sample. To analyse the unit cell parameters of the sample the profile fitting is also done using FullProf program, see Fig 3.1(b). For the Le-bail fittings, some of the important parameters selected in the FullProf program are; Peak Shape: Pseudo-Voigt, Background Mode: Linear interpolation between a set of background points with refinable heights, General information on phase: Calculation- Profile Matching with constant scale factor, Symmetry operation: Generated automatically from the symbol. The unit cell parameters of the $CaMoO_4$ power sample are tabulated in Table 3.1.

Although the diffraction peak positions of SCM, SCEY, and CCEY are nearly identical confirming structural similarity differences in peak sharpness and intensity are observed. These variations are attributed to the synthesis method, which affects the particle size and crystallinity. Specifically, the solid-state reaction method (SCM and SCEY) produces sharper and more intense peaks due to larger particle sizes and better crystallinity. In contrast, the CCEY sample exhibits slightly broadened peaks, indicating reduced crystallite size and increased microstrain, consistent with the nature of combustion synthesis.

These subtle differences are not indicative of a phase change but rather reflect differences in morphology and crystallite size. The retention of the tetragonal structure across all samples demonstrates the robustness of the $CaMoO_4$ host lattice, even with $Er^{3+}/Yb^{3+}$ doping and varying synthesis methods.

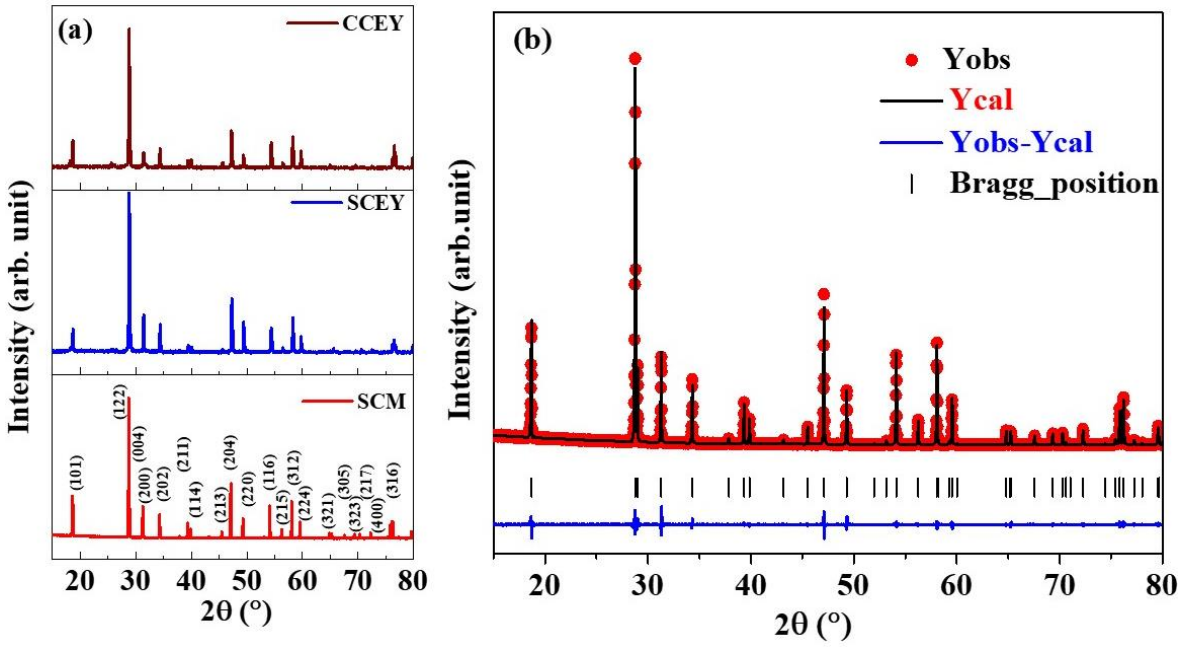


*Figure 3.1* ***(a)*** *XRD pattern of CCEY, SCEY and SCM, and* ***(b)*** *Le-bail fit of SCM.*

*Table 3.1 The unit cell parameters of $CaMoO_4$ powder (SCM) obtained by Le-bail fitting*

| Parameter | Value |
|---|---|
| Name | $CaMoO_4$ |
| Structure | Tetragonal |
| Space group | $I4_1/a$ (88) |
| Unit cell parameters: | |
| a, b, and c | 5.2241(0) Å, 5.2241(0) Å and 5.4292(2) Å |
| $\boldsymbol{\alpha=\beta=\gamma}$ | 90 ° |
| Volume | 148.17545(3) $Å^3$ |
| $R_p$ | 13.6 |
| $R_{wp}$ | 14.3 |
| $R_{exp}$ | 8.59 |
| $\chi^2$ | 2.78 |

Further, the appearance of sharper peaks in case of conventional solid-state reaction method is due to the large particle sizes of the powder sample. This is also confirmed by the

TEM analysis of the samples. The bulky nature of particles is observed in case of solid-state reaction synthesis route, whereas, nanoparticles are observed for the samples synthesized via solution combustion method shown in Fig 3.2(a) and 3.2(b), respectively. Hence XRD peaks of the $CaMoO_4$ powder sample are sharp for solid-state reaction synthesis routes relative to the solution combustion method synthesized sample. Elemental mapping of the SCEY and CCEY sample are shown in Fig 3.2(c) and 3.2(d), respectively. The presence of the elements Er, Yb, Ca, Mo, and O in the elemental mapping confirm that the successful doping of the $Er^{3+}$ and $Yb^{3+}$ in $CaMoO_4$ host.

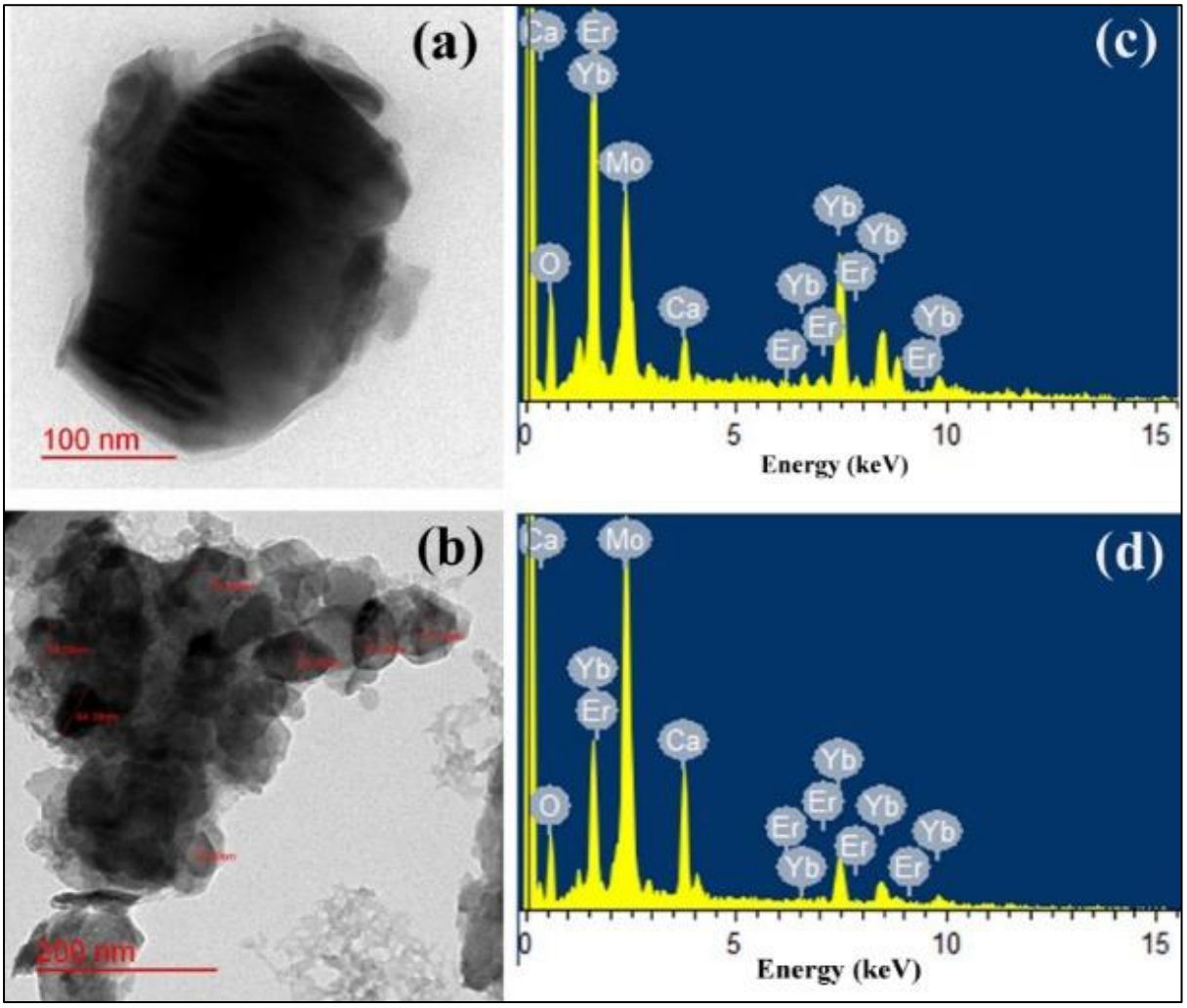


*Figure 3.2 TEM image of **(a)** SCEY, and **(b)** CCEY. Elemental mapping of **(c)** SCEY, and **(d)** CCEY.*

### 3.3.2 FTIR and Raman measurements: Vibrations and lattice phonon frequency analysis

The FT-IR spectra of all the three samples i.e., SCM, SCEY and CCEY are shown in Fig 3.3. The spectra show identical vibration patterns for all the three phosphors, although the band intensities are different. The FT-IR spectra of SCM and SCEY display different bands occurring at 434, 750, 806, 996, 1042, 1556, 1971, 2151 and 2354 $cm^{-1}$ [116]. The sharp peak observed at 434 $cm^{-1}$ is due to anti-symmetric bending vibration of Mo–O bonds whereas the intense absorption bands at 750 and 806 $cm^{-1}$ are characteristics of antisymmetric stretching vibrations of O-Mo-O in the $[MoO4]^{2-}$ tetrahedron in the crystal [33][34]. Asymmetric stretching mode of the adsorbed $CO_2$ appears at 2354 $cm^{-1}$ [117] while the O-H bending vibration of water appears at 1556 $cm^{-1}$. The 2354 $cm^{-1}$ band is missing in the CCEY phosphor due to the fact the preparation of this sample occurred at a relatively high temperature (450 $^{\circ}C$).

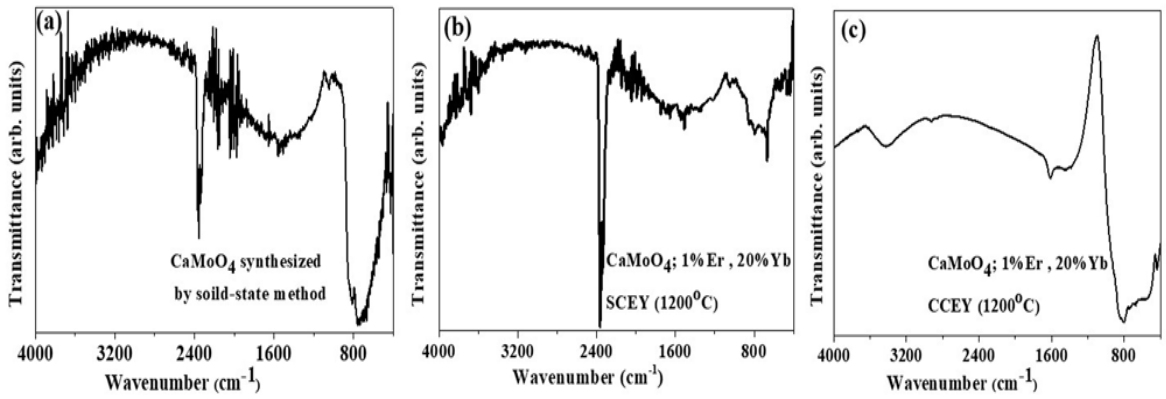


*Figure 3.3 Fourier transforms infrared spectrum for **(a)** SCM, **(b)** SCEY, and **(c)** CCEY.*

The characteristics vibrational modes of the synthesized sample SCM is also identified using the Raman spectum in the range from 100-1000 $cm^{-1}$, as shown in Fig 3.4. The obatained Raman spectrum is same as the previouly reported scheelite type structure [118]. The scheelite

structured compounds display vibrational modes which can be charcterized in two groups as- (i) modes due to internal vibrartions, that are due to vibrations inside the $[MoO_4]^{2-}$ molecular units, and (ii) modes due to external vibrations, which are due to lattice vibrations of $Mo^{2+}$ metal ions and rigid $[MoO_4]^{2-}$ units. Group theory calculations indicate 26 different vibration modes for molybdates having a scheelite-type tetragonal structure as is given in Eq. (3.1) [119]

$$\Gamma_{[(\text{Raman})+(\text{Infrared})]} = \left(3A_g + 5B_g + 5E_g\right) + (5A_u + 3B_u + 5E_u) \quad \ldots (3.1)$$

where, $A_g$, $B_g$, and $E_g$ are Raman active vibrational modes which arise due to identical motion of the clusters in the $CaMoO_4$ lattice. Herein, *A* and *B* modes are nondegenerate, whereas, the *E* modes are doubly degenerate. Among the 8 vibrational modes which appear in the Raman spectrum of pure $CaMoO_4$, the most intense mode is observed at 883 $cm^{-1}$. This band is due to symmetric vibrations of Mo-O stretching mode and assigned to $\nu_{s(1)}(A_g)$ (Mo-O). Another peak at 851 $cm^{-1}$ is the antisymmetric stretching mode, $\nu_{as(3)}(B_g)$ (Mo-O). Similarly, the other modes $\nu_3(E_g)$, $\nu_4(E_g)$, and $\nu_4(B_g)$ are, respectively, observed at 797, 408, and 397 $cm^{-1}$. The doubly degenerated modes $\nu_2(A_g+B_g)$ appear around 328 $cm^{-1}$. All spectra were normalized to the main peak at 883 $cm^{-1}$ (called peak A) as it is less influenced by the beam orientation [120].

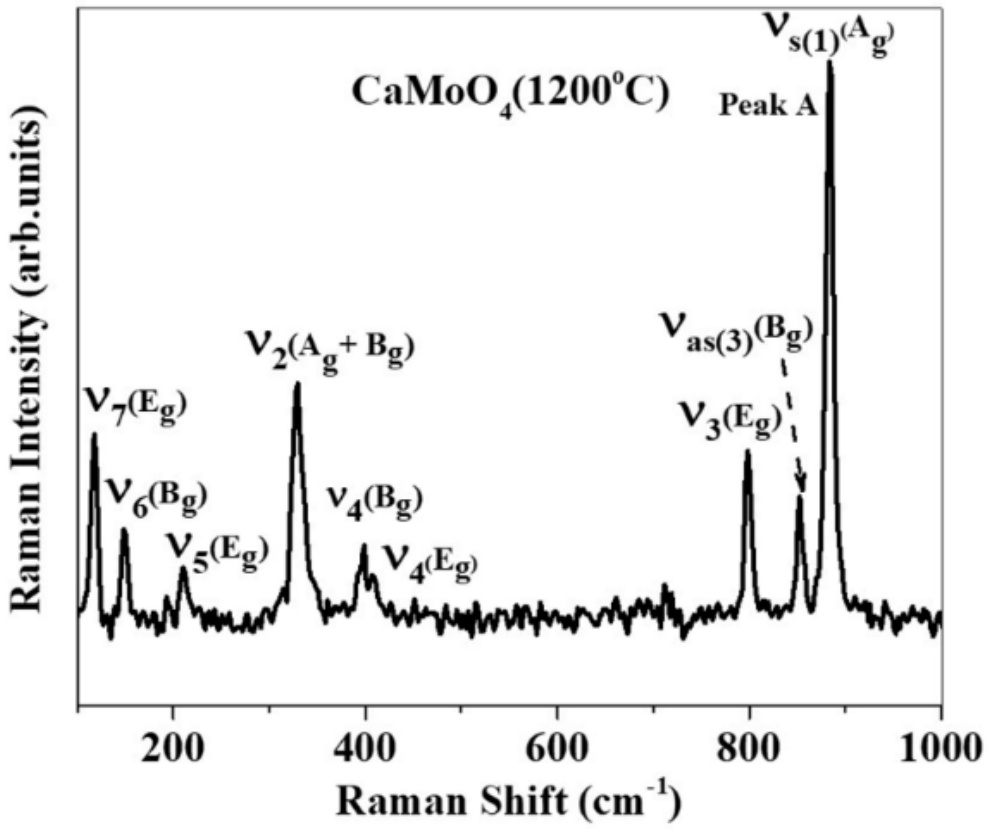


*Figure 3.4 Raman spectrum of $CaMoO_4$ powder sample synthesized by solid state reaction method.*

## 3.4 Luminiescence studies

### 3.4.1 Photo-luminiescence excitation and emission

The photoluminescence (PL) emission and excitation spectra of SCM, SCEY, and CCEY samples are shown in Fig 3.5. The SCM sample (pristine $CaMoO_4$) shows a broad excitation spectrum in the ultraviolet (UV) region peaking at 312 nm. This broad peak is due to the charge transfer transition (CTB) between the $O^{2-}$ and $Mo^{6+}$ ligands [121]. The presence of intense CTB indicates the possibility of an energy transfer from $MoO^{4-}$ moieties to $Er^{3+}$ ions. The excitation spectra of SCEY and CCEY samples do not show excitation band in the UV region (negligibly weak) while there appear sharp and intense excitation peaks at 365, 378,

405, 450, and 488 nm which are assigned to $^4I_{15/2} \rightarrow {}^4G_{9/2}$, $^4I_{15/2} \rightarrow {}^4G_{11/2}$, $^4I_{15/2} \rightarrow {}^2H_{9/2}$, and $^4I_{15/2} \rightarrow {}^4F_{5/2}$ transitions, respectively in $Er^{3+}$ ions. These electronic transitions of $Er^{3+}$ ions are due to intra-configurationally f-f transitions of $Er^{3+}$ ions.

Fig 3.5(b) shows the PL emission of SCM, SCEY, and CCEY samples under 312, 378, and 378 nm excitation, respectively. The emission spectra of pure $CaMoO_4$ shows a wide range from 400 to 600 nm in the visible region. The emission spectra of SCEY and CCEY phosphors contain three characteristic peaks centred at 407 nm, 531 nm and 553 nm corresponding to $^2H_{9/2} \rightarrow {}^4I_{15/2}$, $^2H_{11/2} \rightarrow {}^4I_{15/2}$, and $^4S_{3/2} \rightarrow {}^4I_{15/2}$ transitions, respectively of $Er^{3+}$ ion. Herein, $Yb^{3+}$ ion acts as a sensitizer for $Er^{3+}$ ions. Among all the emission bands, the PL emission intensity of the $^4S_{3/2} \rightarrow {}^4I_{15/2}$ electronic transition is the maximum, which is the characteristic green emission. The peak positions for all the emission peaks for both the doped phosphors are the same. However, the emission peaks intensity for the sample CCEY is relatively high compared to SCEY.

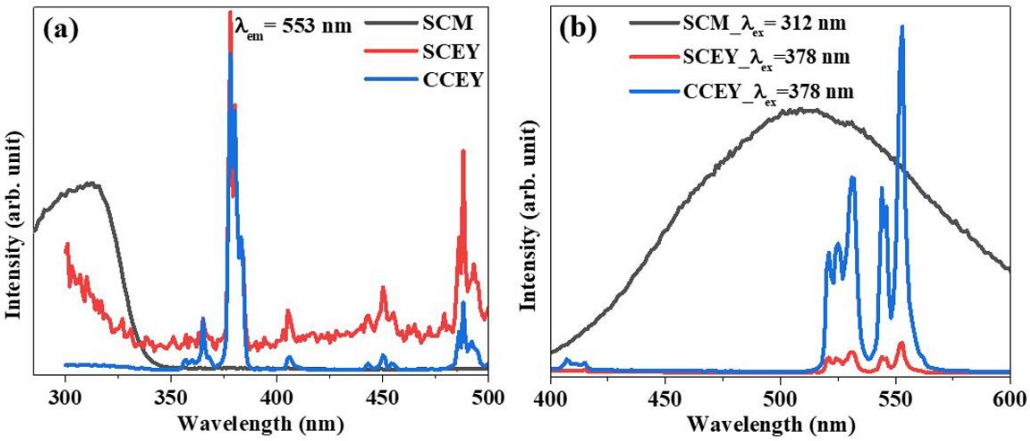


*Figure 3.5* ***(a)*** *excitation spectra, and* ***(b)*** *emission spectra of SCM, SCEY, and CCEY samples.*

## 3.4.2 Photon upconversion emission

The UC spectra of the $Ca_{1-x-y}Er_xYb_yMoO_4$ synthesized by solid-state reaction method are shown in Fig 3.6(a). The $Er^{3+}$ contents ($x$) have been varied from 0.004 to 0.015 with a fixed

$Yb^{3+}$ (y=0.2) concentration. The UC luminescence spectra exhibited two strong emission bands at 531 nm and 552 nm, corresponding to the $^2H_{11/2} \rightarrow {}^4I_{15/2}$ and $^4S_{3/2} \rightarrow {}^4I_{15/2}$ transitions, respectively. While, two other relatively weak emission bands at 657 nm and 670 nm corresponding to the $^4F_{9/2} \rightarrow {}^4I_{15/2}$ transition are also observed [122]. Initially the UC emission intensity increases with increasing the concentration of $Er^{3+}$ ions from x=0.004 to 0.01, reaching a maximum value at x=0.01. The UC emission intensity of the SCEY sample decreases, after a further increase of $Er^{3+}$ concentration beyond the optimized sample, due to concentration quenching effect of rare-earth ions at higher concentrations [123]. This happens due to the decreased distance between $Er^{3+}$ and $Yb^{3+}$-ions at higher $Er^{3+}$ concentration [123]. Due to smaller distance an energy transfer between nearest $Er^{3+}$/ $Er^{3+}$ and $Yb^{3+}$/$Er^{3+}$ ions occur. This basically due to non-radiative energy transfer either due to multipole-multipole interactions or due to an exchange interaction. A similar result is also seen with other host matrices doped with $Er^{3+}$ or co-doped with $Er^{3+}$/ $Yb^{3+}$[124]. So, from here we can conclude that $Ca_{0.79}$ $Er_{0.01}Yb_{0.2}MoO_4$ is our optimized sample among series of $Er^{3+}$/ $Yb^{3+}$ co-doped $CaMoO_4$. When we compare the UC emission intensity for SCEY and CCEY samples, the intensity for CCEY sample is thirty times higher compared to CCEY, see Fig 3.6(b).

*Up-Conversion mechanism*: For the analysis of the number of pump photons involved in a particular UC transition the log-log plot of the emission intensities (*I)* vs laser pumping power (*P)tabl* are plotted, see Fig 3.6(c) and Fig 3.6(d). In the up-conversion process, emission intensity $I$ is proportional to the $n^{th}$ power of $P$, that is: $I \propto P^n$[125]. Where, $I$ represent the emission intensity, $n$ is the number of infrared photons required in a single visible photon generation, and $P$ is the laser pumping power. The value of slopes ($n$) for six different fitted lines shown in Fig 3.6(c) for the SCEY sample are 2.01, 2.01, 1.86, 2.03, 1.78,

and 1.68 corresponding to green emissions at 520 nm, 531 nm, 544 nm, and 552 nm, and red emissions at 657 nm and 670 nm, respectively. Similarly, for the CCEY sample, the calculated slopes (*n*) are 1.74, 1.75, 1.62, 1.62, 1.27 and 1.10 at 520, 531, 544 and 552 for green emissions and 657 and 670 nm for red emissions, respectively (see Fig 3.6(d)). The slope values of *n* for both of the samples, i.e., for SCEY and CCEY, imply that the UC phenomenon is the two-photon process for both the green and the red emissions.

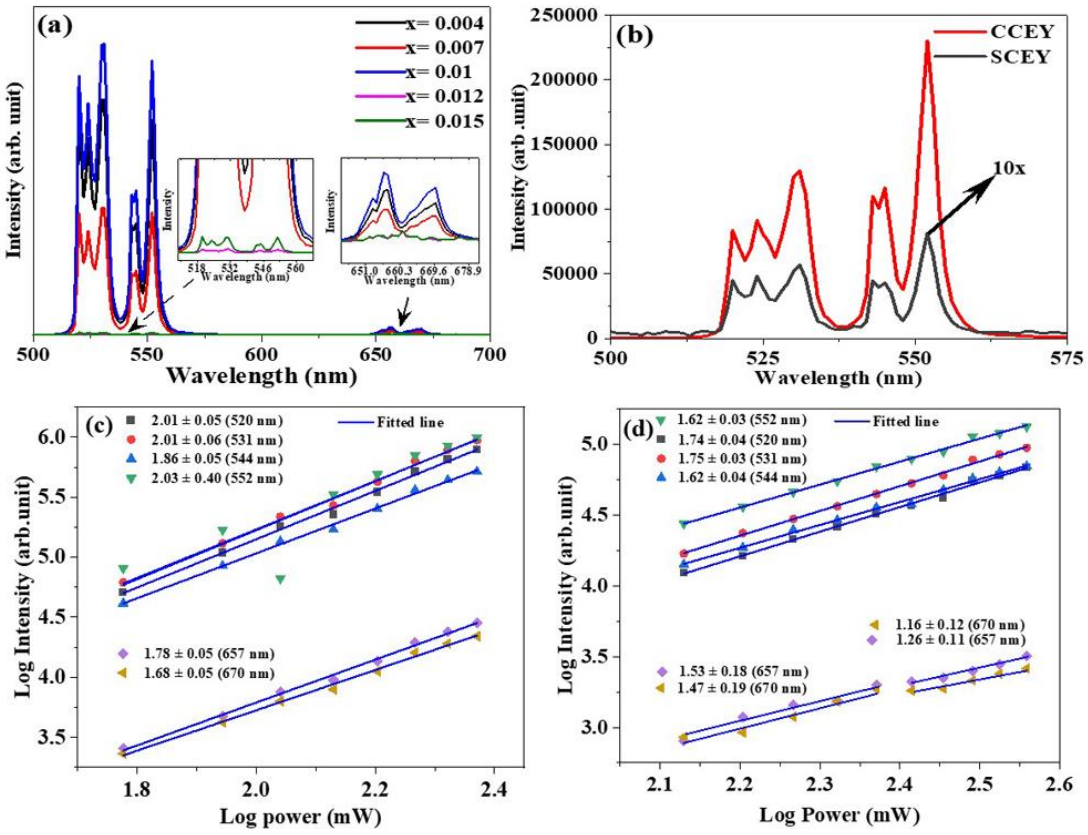


*Figure 3.6* ***(a)*** *UC luminescence spectra of SCEY with a variation in the concentration of* $Er^{3+}$. ***(b)*** *comparison of UC emission spectra of SCEY and CCEY. Log-log plot of UC emission intensity vs. laser input power for* ***(c)*** *SCEY, and* ***(d)*** *CCEY.*

The detailed explanation of the UC mechanism induced via two-photon process in the $Er^{3+}$/ $Yb^{3+}$ co-doped $CaMoO_4$ has been summarized in the partial energy level diagram shown in Fig 3.7 and explained in detailed in our earlier works [126]. The absorption of 980 nm excitation in the ground state of $Er^{3+}$ and $Yb^{3+}$ ions result in the promotion of ions into the

$^4I_{11/2}$ and $^2F_{5/2}$ excited states. respectively. Due to the non-radiative relaxation process, some of the $Er^{3+}$-ions move to the $^4I_{13/2}$ from the $^4I_{11/2}$ state. Now there are two possibilities of transition: first, each $Er^{3+}$ ions promote from the $^4I_{11/2}$ and $^4I_{13/2}$ states into the $^4F_{7/2}$ and $^4F_{9/2}$ states by continuous absorption of 980 nm photon. The transitions occur from excited states of $Er^{3+}$ -ion, this process is called excited state absorption (ESA). Second, the energy transfers of excited $Yb^{3+}$ ions to its adjacent $Er^{3+}$ ions in the $^4I_{15/2}$ ground state to the $^4I_{11/2}$ state. Also, the fast energy transfer occurs from the $^2F_{5/2}$ level of $Yb^{3+}$ to the $^4I_{11/2}$ of $Er^{3+}$-ion directly. The populated ions in the level $^4I_{11/2}$ of $Er^{3+}$-ion transits to the level $^4F_{7/2}$ of $Er^{3+}$-ion by subsequent absorption of 980 nm. The transition $^4F_{7/2}\rightarrow{}^2H_{11/2}$ and $^4F_{7/2}\rightarrow{}^4S_{3/2}$ occur due to the rapid non-radiative relaxation (NR) because of the small energy gap between these levels [127]. The transitions from the $^2H_{11/2}\rightarrow{}^4I_{15/2}$ produce 520, 531 and $^4S_{3/2}\rightarrow{}^4I_{15/2}$ of $Er^{3+}$ produce 544, and 552 nm green emissions, respectively. The radiative transition from $^4F_{9/2} \rightarrow {}^4I_{15/2}$ leads to the red emission of wavelength 657 nm and 670 nm. Additionally, non-radiative transitions $^2H_{11/2}\rightarrow{}^4F_{9/2}$ and $^4S_{3/2}\rightarrow{}^4F_{9/2}$ in $Er^{3+}$-ions are also possible.

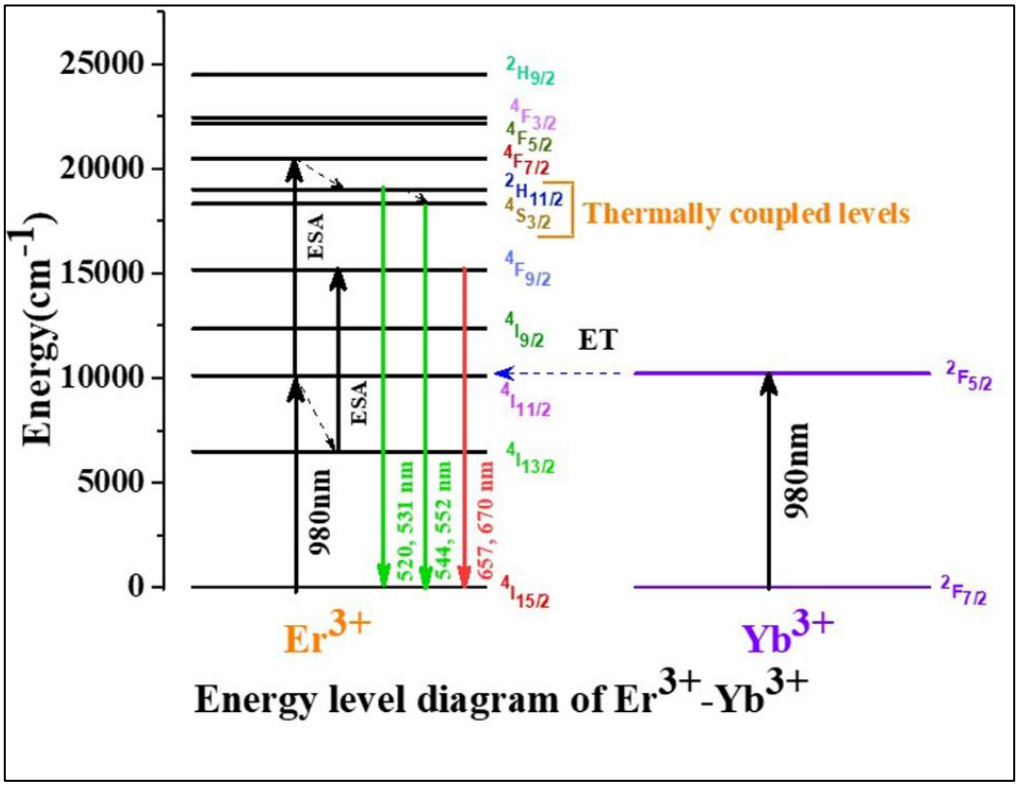


*Figure 3.7 Schematic energy level diagram showing UC mechanism in $Er^{3+}$/ $Yb^{3+}$ co-doped $CaMoO_4$.*

## 3.5 Temperature-dependent up-conversion: Optical temperature sensing application

A comparative study of the temperature-dependent UC emission of the optimized $Ca_{0.79}Er_{0.01}Yb_{0.2}MoO_4$ synthesized by solid-state reaction method and gel-combustion method are performed. Both the sample are calcined at 1200 $^{\circ}$ C for the comparative study. The 980 nm continuous wave laser source at a low laser power of 24 mW has been used for the excitation to avoid significant heating by the source itself. Although a K-type thermocouple was used to monitor and validate the temperature near the phosphor during measurements, it did not make direct contact with the luminescent region of the sample. The primary focus of this study is on demonstrating a non-contact optical thermometry approach, where the temperature is inferred through fluorescence intensity ratio (FIR) measurements between thermally coupled levels of $Er^{3+}$ ions. This luminescence-based sensing method does not

require physical contact between the detection system and the sample, highlighting its potential for remote temperature sensing in challenging environments. The temperature ranges from 305 K - 573 K has been used for observing the UC emission spectra in the wavelength range 500 nm - 575 nm. The UC emission intensity depends on the host and the lanthanide doping. If the phonon frequency of the host is low the UC emission intensity will be higher because the lower phonon frequency results in minimum non-radiative transitions [128][49]. The temperature dependent multi-phonon non-radiative decay as a function of energy gap and temperature can be defined as.

$$W_{NR}(T) = W_{NR}(0)\left(1 - e^{-h\nu/kT}\right)^{-n} \quad \ldots (3.1)$$

Where, $W_{NR}(T)$ and $W_{NR}(0)$ are the non-radiative decay rates at any temperatures T and 0 K, respectively. The motivation/reason of the analysis of the temperature-dependent up-conversion spectra is due to the energy difference between the $^2H_{11/2}$ and $^4S_{3/2}$ states of the $Er^{3+}$ ion is ~735.34 $cm^{-1}$[129]. Hence, it is possible to get a population redistribution with thermal excitation. We have plotted fluorescence intensity ratio (FIR) vs. temperature as shown in Fig 3.8(a).

FIR theoretically can be explained by Boltzmann's distribution formulated as [130].

$$FIR = \frac{I_{531}\left(^2H_{11/2} \rightarrow {}^4I_{15/2}\right)}{I_{553}\left(^4S_{3/2} \rightarrow {}^4I_{15/2}\right)} = \frac{W_H g_H h\nu_H}{W_S g_S h\nu_S} exp\left(\frac{-\Delta E}{k_B\, T}\right) \quad \ldots (3.2)$$

$$= Bexp\left(\frac{-\Delta E}{k_B\, T}\right) \quad \ldots (3.3)$$

Where, $I_{531}$ and $I_{553}$ are the integrated intensities corresponding to $^2H_{11/2} \rightarrow {}^4I_{15/2}$ ($\sim 523 - 531$ nm) and $^4S_{3/2} \rightarrow {}^4I_{15/2}$ ($\sim 544 - 553$ nm) bands of $Er^{3+}$-ion, respectively. $g_H$ and $g_S$ are the (2J+1) degeneracies of the levels $^2H_{11/2}$ and $^4S_{3/2}$. The $W_H$ and $W_S$ are the

radiative probabilities and $h\nu_H$ and $h\nu_S$ are the photon energies of $^2H_{11/2} \rightarrow {}^4I_{15/2}$ and $^4S_{3/2} \rightarrow {}^4I_{15/2}$ transitions due to the spontaneous emission, respectively. ΔE is the energy gap between the two thermally coupled emitting levels, $k_B$ is the Boltzmann constant and $T$ is the absolute temperature.

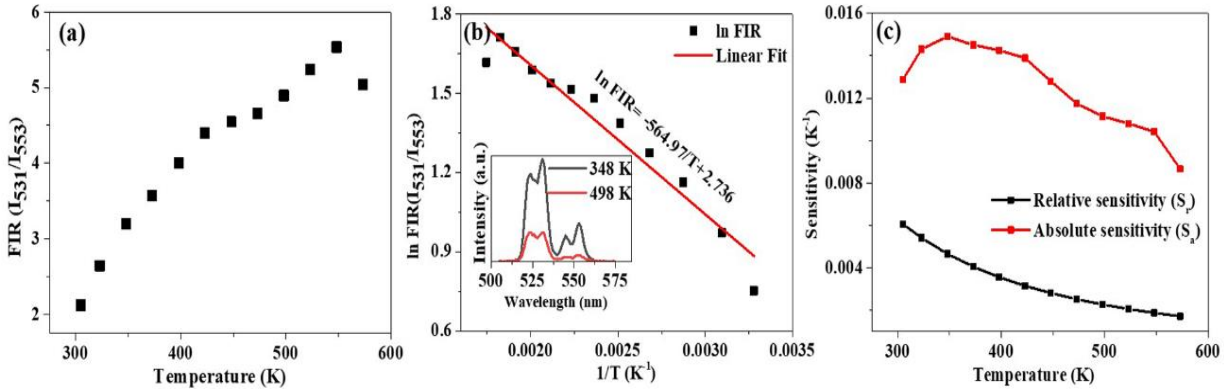


*Figure 3.8* ***(a)*** *Green emission FIR ($I_{531}/I_{553}$) vs. temperature plot,* ***(b)*** *the ln FIR ($I_{531}/I_{553}$) vs. inverse absolute temperature plot of $Er_{0.01}Yb_{0.2}Ca_{0.79}MoO_4$ synthesized by the solid-state method (the UC spectra of the green band at 348 K and 498 K are shown in inset).* ***(c)*** *The plot of relative sensitivity and absolute sensitivity as a function of the temperature of $Er_{0.01}Yb_{0.2}Ca_{0.79}MoO_4$ synthesized by the solid-state method.*

The FIR value increases from 2.12 to 5.54 monotonically as temperature increases from 305 K to 548 K. Increasing the temperature beyond 548 K, the UC emission peaks become noisy due to the thermal quenching effect and it is difficult to measure FIR value. The energy band-gap between two thermally coupled levels ($^2H_{11/2}$ *and* $^4S_{3/2}$) can be calculated by taking log on both sides in equation (3.3).

$$ln(FIR) = ln(B) + \left(-\frac{\Delta E}{k_B T}\right) = \ln(B) + \left(-\frac{C}{T}\right) \qquad \ldots (3.4)$$

where, the unknown constants B and C need to be calculated. The constant value B depends on the characteristics of the prepared phosphor such as degeneracy ($g_H$ and $g_S$) and spontaneous emission probability ($W_H$ and $W_S$) and the response of the detection system. We are interested in spontaneous emission probabilities ($W_H$ and $W_S$), so they are considered as most sensitive variables. The FIR depends on the average phonon frequency of the host

materials and the change in the host material may change the value of energy difference $\Delta E$. The equation (3.4) is fitted in linear form in the ln (FIR) vs. inverse of temperature (1/T) graph (as shown in Fig 3.8(b) and Fig 3.9(b)). The value of the slope and the intercept for the SCEY and CCEY are (564.97 ± 43.56, 2.73 ± 0.11) and (836.84 ± 14.51, 3.25 ± 0.04), respectively. By using the above-calculated value of the slope, the energy-gap between thermally coupled levels ($^2H_{11/2}$ and $^4S_{3/2}$) is found 392.67 $cm^{-1}$ and 581.62 $cm^{-1}$ for SCEY and CCEY samples, respectively.

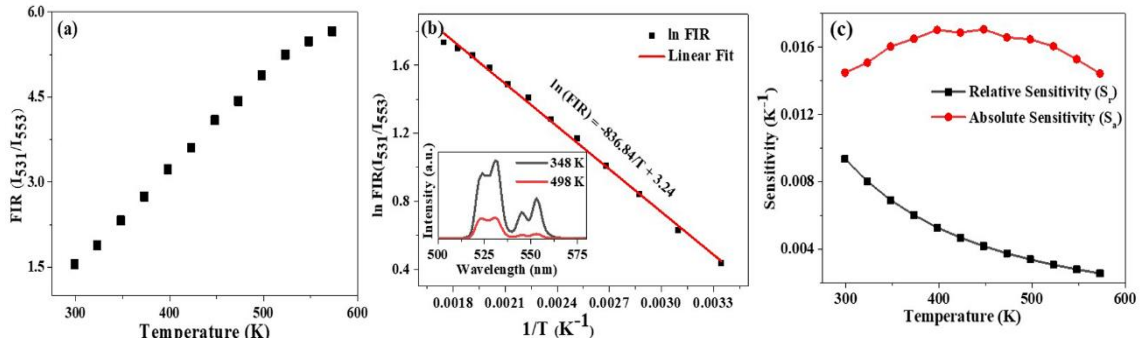


*Figure 3.9* ***(a)*** *Green emission FIR ($I_{531}/I_{553}$) vs. temperature plot,* ***(b)*** *the ln FIR ($I_{531}/I_{553}$) vs. inverse absolute temperature plot of $Er_{0.01}Yb_{0.2}Ca_{0.79}MoO_4$ synthesized by the gel-combustion method (the UC spectra of the green band at 348 K and 498 K are shown in inset).* ***(c)*** *The plot of relative sensitivity and absolute sensitivity as a function of the temperature of $Er_{0.01}Yb_{0.2}Ca_{0.79}MoO_4$ synthesized by the gel-combustion method*

The main property of any good optical sensor is that it detects/senses slight temperature change. Therefore, the other parameters like relative sensitivity ($S_r$) and absolute sensitivity ($S_a$) have been also calculated for standard verification of sensitivity of the prepared phosphors. Mathematically, the absolute sensitivity ($S_a$) can be defined as the rate of change of the FIR with the variation in the temperature and is given as [131].

$$S_a = \frac{\partial(FIR)}{\partial T} = FIR \times \frac{\Delta E}{k_B T^2} \qquad \ldots (3.5)$$

Relative sensitivity ($S_r$) is the ideal parameter for comparing the sensitivity of the material and is given as,

$$S_r = \frac{1}{(FIR)} \times \frac{\partial(FIR)}{\partial T} = \frac{\Delta E}{k_B T^2} \qquad \ldots (3.6)$$

Where, all the above terms have been already elaborated earlier. From the above formulas, it can be depicted that the sensitivity of the prepared phosphors is higher if the energy gap of the two thermally coupled levels is high. The plot of $S_a$ and $S_r$ against increasing temperature for both the samples i.e., SCEY and CCEY are shown in Fig 3.8(c) and Fig 3.9(c), respectively. The pattern of the absolute sensitivity for both the samples with increasing temperature initially increases and reached to a maximum value at a certain temperature, and then it starts decreasing. Here it is notable that, the amplification factor for the thermal sensitivity is represented by the ratio of transition probabilities from the emitting levels. The maximum relative sensitivity of the phosphors SCEY and CCEY are 0.0061 $K^{-1}$ at 305 K and 0.0094 $K^{-1}$ at 299 K, respectively. While the maximum absolute sensitivities for the phosphors SCEY and CCEY are 0.0150 $K^{-1}$ at 348 K, and 0.0170 $K^{-1}$ at 398 K, respectively. The sensitivity of CCEY is higher than the SCEY phosphor. This indicates that the prepared $Ln^{3+}$-doped $CaMoO_4$ is useful in temperature sensing applications.

## 3.6 Conclusions

In summary, in this chapter, the pristine and $Er^{3+}$, $Yb^{3+}$ co-doped $CaMoO_4$ phosphor using solid state reaction and solution combustion methods have been successfully synthesized. The intensity of the emission peaks synthesized using solution combustion method is about thirty times higher than the sample synthesized using solid state reaction method. The same trend is observed for the upconversion emission also under the 980 laser excitations. Temperature dependent UC emission study suggests that the materials are ideal to sense the temperature by making use of fluorescence intensity ratio of the transitions taking place from $^4S_{3/2}$ and

$^2H_{11/2}$ state of $Er^{3+}$ ion to its ground state. The maximum relative sensitivity of the phosphors synthesized by solid state reaction method and solution combustion method are 0.0061 $K^{-1}$ at 305 K and 0.0094 $K^{-1}$ at 299 K, respectively. Whereas, the absolute sensitivity for them obtained are 0.0150 $K^{-1}$ at 348 K, and 0.0170 $K^{-1}$ at 398 K, respectively. Hence, solution combustion method synthesized phosphor shows better temperature sensitivity as compared to the solid-state reaction method-based phosphor. This material can be explored for the non-contact based optical temperature sensor.

.